Progress In Electromagnetics Research B, Vol. 72, 49–65, 2017

Analytical Calculations of Electromagnetic Quantities for Slotted Brushless Machines with Surface-Inset Magnets

Akbar Rahideh[1], Hossein Moayed-Jahromi[2], Mohamed Mardaneh[1], Frédéric Dubas[3, *], and Theodosios Korakianitis[4]

Abstract—In this paper, two-dimensional (2-D) analytical magnetic field calculations are used to compute crucial quantities of Brushless permanent-magnet (PM) machines with surface-inset PMs. The analytical magnetic field distribution is based on the subdomain technique in which the slotting and tooth-tip effects have been considered. It includes both different magnetization patterns (e.g., radial, parallel and Halbach) and different spatial distribution of winding (e.g., concentrated and distributed with one or more layers). The saturation effect of the magnetic circuit is neglected. In this investigation, the phase and line induced back electromotive force (EMF) waveforms, electromagnetic/cogging/reluctance torques, self-/mutual-inductances and unbalanced magnetic forces (UMFs) have been analytically calculated. The analytical expressions can be used for Brushless machines having surface-inset PMs with any radius-independent magnetization pattern. In this study, two slotted Brushless PM machines with surface-inset PMs have been selected to evaluate the efficacy of the analytical expressions by comparing the results with those obtained by the finite-element method (FEM). One of the case studies is a 9-slots/8-poles Brushless DC (BLDC) machine with radially magnetized PMs, non-overlapping all teeth wound winding and six-step rectangular armature current waveforms. The other is a 15-slots/4-poles Brushless AC (BLAC) machine with Halbach magnetization PMs, double-layer overlapping winding and sinusoidal armature current waveforms.

1. INTRODUCTION

High energy density PMs such as samarium-cobalt and neodymium-iron-boron have paved the way for the widespread applications of Brushless PM machines in high performance drive systems. Before the advent of rare-earth PMs, Brushless PM machines had no chance to compete with their main rival, i.e., induction machines. In general, high performance drive systems are desired to have some or all of the following features: high efficiency, high energy density per unit volume, low torque ripple, no or minimal saturation occurrence, low vibrations, low acoustic noise pollution, minimum harmonic generation, minimum development of UMFs, high reliability, rugged structure, ability to operate in adverse conditions and/or hazardous environment, long life-time, minimum maintenance requirement, ability to operate at wide range of speed, possibility to be designed for very high-speed applications, high fault tolerant property, high controllability, robustness, and proper heat removal and cooling system. Some of these features depend on the machine design, some others are dependent on the control design and some of them are influenced by both the machine and control design. Since some of these features are in conflict, designing a drive system to possess all of the above-mentioned properties is a challenging

Received 15 September 2016, Accepted 15 December 2016, Scheduled 3 January 2017
* Corresponding author: Frederic Dubas (FDubas@gmail.com).
[1] Department of Electrical and Electronics Engineering, Shiraz University of Technology, Shiraz, I.R., Iran. [2] Fars Regional Electrical Company (FREC), Shiraz, Iran. [3] Département ENERGIE, FEMTO-ST, CNRS, Univ. Bourgogne Franche-Comté, Belfort, France. [4] Parks College of Engineering, Aviation and Technology, Saint Louis University, Saint Louis, MO 63013, USA.

issue. Therefore depending on the application of the drive system, the features are prioritized and the design process is carried out based on the prioritization.

According to the prioritized features, the most suitable topology of the Brushless PM machine (i.e., slotless/slotted, inner/outer rotor, surface-mounted/surface-inset/interior PMs) is selected. For example, if a very high-speed machine is required, a machine with slotless stator structure is selected. Basically at normal speed operation, the slotted stator structure outperforms the slotless one in terms of higher energy density per unit volume due to the lower effective air-gap in the former compared to that of the latter. On the other hand, the slotless stator structure results in zero cogging torque and very low armature reaction which are important for high-speed applications. There are four main possible PM topologies: i) surface-mounted; ii) surface-inset; iii) radial interior (a.k.a. spoke or circumferential flux interior PMs) and iv) circumferential interior (a.k.a. buried or radial flux interior PMs). Among them, the interior offers the highest mechanical robustness and lowest PM eddy-current losses at the expense of higher cost. In contrast, the surface-mounted PMs structure is less expensive but suffers from low mechanical robustness and high PM eddy-current losses. A trade-off between these two options is the surface-inset PMs topology in which the mechanical robustness is higher and PM eddy-current losses are lower than that of the surface-mounted PMs and the cost is lower compared to interior PMs structures.

For the design and analysis purpose of Brushless PM machines, their model is a prerequisite. The model of an electric machine can be dynamic or static in which each can be analytic [1–33] or numeric [34–36]. For design purposes, normally, static model is sufficient and the analytic model, if possible, is preferred over the numeric one. The analytic model of a Brushless PM machine can be obtained via different approaches such as [37]: i) magnetic equivalent circuit; ii) Schwarz-Christoffel mapping method and ii) Maxwell-Fourrier methods (i.e., multi-layers models and subdomain technique). The latter is far more accurate than the former and can be used to almost precisely calculate crucial quantities such as the magnetic field distribution, cogging/reluctance/instantaneous torques, back EMF waveforms, self-/mutual-inductances and UMFs.

2-D analytical magnetic field calculations have been reported for both surface-mounted [1–23] and surface-inset PMs [23–31] in which some of them deal with the slotless stator structure [1–28] and some others investigate the slotted stator structure [7–31]. Analytical magnetic field expressions have been utilized to calculate the PM eddy-current loss with(out) the current penetration effect [4, 14, 28], cogging torque [13, 32], reluctance torque, instantaneous torque [27, 30], back EMF waveforms [5, 24, 27], self-/mutual-inductances [2, 27], and UMFs [5, 33].

In this paper, 2-D analytical magnetic field expressions are employed to calculate the cogging/reluctance/instantaneous torques, back EMF waveforms, self-/mutual-inductances and UMFs in the slotted Brushless machines with surface-inset PMs.

2. MAGNETIC FIELD CALCULATIONS

Consider the slotted Brushless machine equipped with surface-inset PMs having p pole pairs and Q slots shown in Figure 1. The winding can be non-overlapping in which the non-overlapping type can be classified as all teeth wound or alternate teeth wound as depicted in Figure 2.

The 2-D magnetic field distribution can be analytically calculated for slotted Brushless machines with surface-inset PMs. To this end, a number of assumptions, as listed in [31], need to be made to either permit or facilitate the analytical solution. According to the infinite permeability assumption of the stator and rotor back-iron, the machine geometry is divided into four active subdomains [see Figure 1]: slots; slot-openings; air-gap; and PMs denoted respectively by sl, so, a, and m. Therefore, the number of subregions with non-overlapping windings [see Figure 2(a) and Figure 2(b)] is $2Q+2p+1$. In the case of double -layer overlapping windings [see Figure 2(c)] each slot is radilly divided into two subregions and instead of index sl, indices slt and slb are used for the top and bottom parts of the slots. Subsequently, the number of subregions will be $3Q + 2p + 1$. The excitation of the system is both armature currents or/and PMs which represented by their Fourier series expansion [31].

Based on Maxwell's equations and the assumptions made, the radial and tangential components of the magnetic flux density in all regions can be calculated by the following expressions where subscripts r and θ denote the radial and tangential components respectively. The superscripts sl, so, a, and m are used to distinguish between different subdomains and $k = 0, 1, \ldots, 2p - 1$ is the PM index and

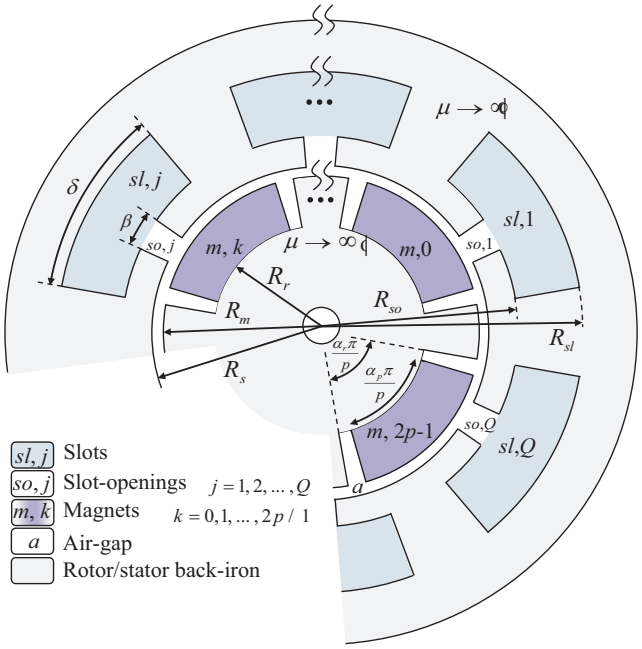

Figure 1. Illustrative representation of the subdomains. Note that each PM with both airspace regions between the PM and the two iron interpoles are assumed to be one subdomain.

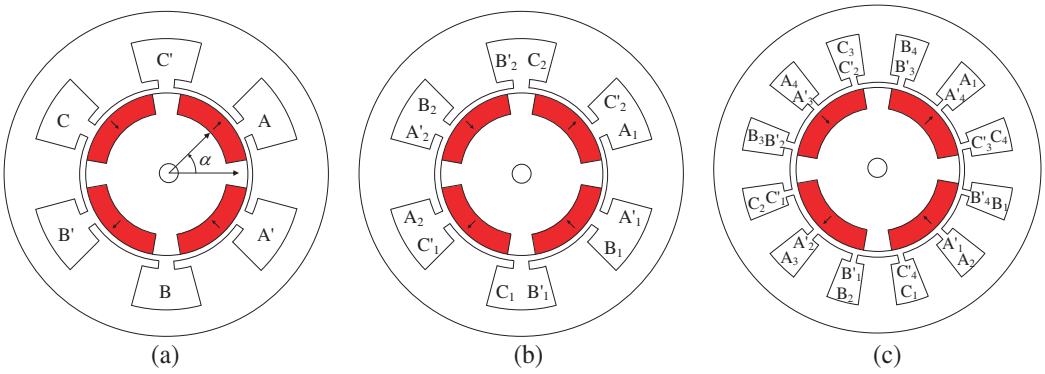

Figure 2. (a) 6-slots/4-poles Brushless PM machines with non-overlapping alternate teeth wound (single layer winding); (b) 6-slots/4-poles Brushless PM machines with non-overlapping all teeth wound (double layer winding); (c) 12-slots/4-poles Brushless PM machines with overlapping full-pitch winding (double layer winding).

$j = 1, 2, \ldots, Q$ is the index of the slots and slot-openings [31].

$$B_r^{m,k}(r,\theta) = -\sum_{w=1}^{W} \frac{wp}{\alpha_r} \left\{ \begin{array}{l} \dfrac{a_w^{m,k}}{R_m} \left[\left(\dfrac{r}{R_m}\right)^{\frac{wp}{\alpha_r}-1} + \left(\dfrac{R_r}{R_m}\right)^{\frac{wp}{\alpha_r}-1} \left(\dfrac{R_r}{r}\right)^{\frac{wp}{\alpha_r}+1} \right] \\ \ldots + \zeta_{w1}^k \left(\dfrac{R_r}{r}\right)^{\frac{wp}{\alpha_r}+1} + k_w^k \end{array} \right\} \sin\left[\frac{wp}{\alpha_r}\left(\theta - \alpha - \frac{k\pi}{p} + \frac{\alpha_r \pi}{2p}\right)\right] \quad (1)$$

$$B_\theta^{m,k}(r,\theta) = -\sum_{w=1}^{W} \left\{ \begin{array}{l} \dfrac{wp}{\alpha_r} \dfrac{a_w^{m,k}}{R_m} \left[\left(\dfrac{r}{R_m}\right)^{\frac{wp}{\alpha_r}-1} - \left(\dfrac{R_r}{R_m}\right)^{\frac{wp}{\alpha_r}-1} \left(\dfrac{R_r}{r}\right)^{\frac{wp}{\alpha_r}+1} \right] \\ \ldots - \dfrac{wp}{\alpha_r} \zeta_{w1}^k \left(\dfrac{R_r}{r}\right)^{\frac{wp}{\alpha_r}+1} + \dfrac{dk_w^k r}{dr} \end{array} \right\} \cos\left[\frac{wp}{\alpha_r}\left(\theta - \alpha - \frac{k\pi}{p} + \frac{\alpha_r \pi}{2p}\right)\right] \quad (2)$$

$$B_r^a(r,\theta) = -\sum_{n=1}^{N} n \left\{ \begin{array}{l} \left[\frac{a_n^a}{R_s}\left(\frac{r}{R_s}\right)^{n-1} + \frac{b_n^a}{R_m}\left(\frac{R_m}{r}\right)^{n+1}\right]\sin(n\theta) \\ \ldots - \left[\frac{c_n^a}{R_s}\left(\frac{r}{R_s}\right)^{n-1} + \frac{d_n^a}{R_m}\left(\frac{R_m}{r}\right)^{n+1}\right]\cos(n\theta) \end{array} \right\} \tag{3}$$

$$B_\theta^a(r,\theta) = -\sum_{n=1}^{N} n \left\{ \begin{array}{l} \left[\frac{a_n^a}{R_s}\left(\frac{r}{R_s}\right)^{n-1} - \frac{b_n^a}{R_m}\left(\frac{R_m}{r}\right)^{n+1}\right]\cos(n\theta) \\ \ldots + \left[\frac{c_n^a}{R_s}\left(\frac{r}{R_s}\right)^{n-1} - \frac{d_n^a}{R_m}\left(\frac{R_m}{r}\right)^{n+1}\right]\sin(n\theta) \end{array} \right\} \tag{4}$$

$$B_r^{so,j}(r,\theta) = -\sum_{u=1}^{U} \frac{\pi u}{\beta}\left[\frac{a_u^{so,j}}{R_{so}}\left(\frac{r}{R_{so}}\right)^{\frac{\pi u}{\beta}-1} + \frac{b_u^{so,j}}{R_s}\left(\frac{R_s}{r}\right)^{\frac{\pi u}{\beta}+1}\right]\sin\left[\frac{\pi u}{\beta}\left(\theta-\theta_j+\frac{\beta}{2}\right)\right] \tag{5}$$

$$B_\theta^{so,j}(r,\theta) = -\frac{b_0^{so,j}}{r} - \sum_{u=1}^{U} \frac{\pi u}{\beta}\left[\frac{a_u^{so,j}}{R_{so}}\left(\frac{r}{R_{so}}\right)^{\frac{\pi u}{\beta}-1} - \frac{b_u^{so,j}}{R_s}\left(\frac{R_s}{r}\right)^{\frac{\pi u}{\beta}+1}\right]\cos\left[\frac{\pi u}{\beta}\left(\theta-\theta_j+\frac{\beta}{2}\right)\right] \tag{6}$$

$$B_r^{sl,j}(r,\theta) = -\sum_{v=1}^{V} \frac{\pi v}{\delta}\left\{ \begin{array}{l} \frac{b_v^{sl,j}}{R_{so}}\left[\left(\frac{R_{so}}{R_{sl}}\right)^{\frac{\pi v}{\delta}+1}\left(\frac{r}{R_{sl}}\right)^{\frac{\pi v}{\delta}-1} + \left(\frac{R_{so}}{r}\right)^{\frac{\pi v}{\delta}+1}\right] \\ \ldots + \frac{\mu_0 J_v^j}{\left(\frac{\pi v}{\delta}\right)^2-4}\left[r - \frac{2R_{sl}}{\frac{\pi v}{\delta}}\left(\frac{r}{R_{sl}}\right)^{\frac{\pi v}{\delta}-1}\right] \end{array} \right\}\sin\left[\frac{\pi v}{\delta}(\theta-\theta_j+\delta 2)\right] \tag{7}$$

$$B_\theta^{sl,j}(r,\theta) = -\left| \begin{array}{l} \frac{\mu_0 J_0^j}{2}\left(\frac{R_{sl}^2}{r} - r\right) \\ \ldots + \sum_{v=1}^{V}\left\{ \begin{array}{l} \frac{\pi v}{\delta}\frac{b_v^{sl,j}}{R_{so}}\left[\left(\frac{R_{so}}{R_{sl}}\right)^{\frac{\pi v}{\delta}+1}\left(\frac{r}{R_{sl}}\right)^{\frac{\pi v}{\delta}-1} - \left(\frac{R_{so}}{r}\right)^{\frac{\pi v}{\delta}+1}\right] \\ \ldots + \frac{2\mu_0 J_v^j}{\left(\frac{\pi v}{\delta}\right)^2-4}\left[r - R_{sl}\left(\frac{r}{R_{sl}}\right)^{\frac{\pi v}{\delta}-1}\right] \end{array} \right\}\cos\left[\frac{\pi v}{\delta}\left(\theta-\theta_j+\frac{\delta}{2}\right)\right] \end{array} \right. \tag{8}$$

where R_r, R_m, R_s, R_{so} and R_{sl} are, respectively, the radii of rotor back-iron, PM, stator bore, slot-opening and slot bottom; θ the spatial angle with respect to the stator fixed reference axis; β the slot-opening span angle; δ the slot span angle; and

$$b_0^{so,j} = \frac{\mu_0 J_0^j}{2}\left(R_{sl}^2 - R_{so}^2\right)\frac{\delta}{\beta} \tag{9}$$

$$k_w^k = -\mu_0\chi_w \left\{ \begin{array}{ll} \frac{\frac{wp}{\alpha_r}M_{rw}^k - M_{\theta w}^k}{\left(\frac{wp}{\alpha_r}\right)^2-1} & for \quad wp \neq \alpha_r \\ \frac{M_{rw}^k - M_{\theta w}^k}{2}\ln r & for \quad wp = \alpha_r \end{array} \right. \tag{10}$$

$$\chi_w = \frac{1-(-1)^w}{2} \tag{11}$$

$$\zeta_{w1}^k = -\mu_0\chi_w \left\{ \begin{array}{ll} \frac{M_{rw}^k - \frac{wp}{\alpha_r}M_{\theta w}^k}{\left(\frac{wp}{\alpha_r}\right)^2-1} & for \quad wp \neq \alpha_r \\ \frac{M_{rw}^k - M_{\theta w}^k}{2}(1+\ln R_r) - M_{\theta w}^k & for \quad wp = \alpha_r \end{array} \right. \tag{12}$$

In the case of *overlapping windings*, the radial and tangential components of the magnetic flux

density in the top and bottom of the slots are expressed as [31]

$$B_r^{slt,j}(r,\theta) = -\sum_{v=1}^{V} \frac{\pi v}{\delta} \frac{b_v^{sl,j}}{R_{so}} \left[\left(\frac{R_{so}}{R_{sl}} \right)^{\frac{\pi v}{\delta}+1} \left(\frac{r}{R_{sl}} \right)^{\frac{\pi v}{\delta}-1} + \left(\frac{R_{so}}{r} \right)^{\frac{\pi v}{\delta}+1} \right] \sin\left[\frac{\pi v}{\delta} \left(\theta - \theta_j + \frac{\delta}{2} \right) \right] \tag{13}$$

$$B_\theta^{slt,j}(r,\theta) = -\left| \begin{array}{l} \dfrac{\mu_0}{2} \left[J_{b0}^j \left(R_{sl}^2 - R_{slm}^2 \right) + J_{t0}^j \left(R_{slm}^2 - r^2 \right) \right] \dfrac{1}{r} \\ \ldots + \displaystyle\sum_{v=1}^{V} \frac{\pi v}{\delta} \frac{b_v^{sl,j}}{R_{so}} \left[\left(\frac{R_{so}}{R_{sl}} \right)^{\frac{\pi v}{\delta}+1} \left(\frac{r}{R_{sl}} \right)^{\frac{\pi v}{\delta}-1} - \left(\frac{R_{so}}{r} \right)^{\frac{\pi v}{\delta}+1} \right] \cos\left[\dfrac{\pi v}{\delta} \left(\theta - \theta_j + \dfrac{\delta}{2} \right) \right] \end{array} \right. \tag{14}$$

$$B_r^{slb,j}(r,\theta) = -\sum_{v=1}^{V} \frac{\pi v}{\delta} \frac{b_v^{sl,j}}{R_{so}} \left[\left(\frac{R_{so}}{R_{sl}} \right)^{\frac{\pi v}{\delta}+1} \left(\frac{r}{R_{sl}} \right)^{\frac{\pi v}{\delta}-1} + \left(\frac{R_{so}}{r} \right)^{\frac{\pi v}{\delta}+1} \right] \sin\left[\frac{\pi v}{\delta} \left(\theta - \theta_j + \frac{\delta}{2} \right) \right] \tag{15}$$

$$B_\theta^{slb,j}(r,\theta) = -\left| \begin{array}{l} \dfrac{\mu_0 J_{b0}^j}{2} \left(\dfrac{R_{sl}^2}{r} - r \right) \\ \ldots + \displaystyle\sum_{v=1}^{V} \frac{\pi v}{\delta} \frac{b_v^{sl,j}}{R_{so}} \left[\left(\frac{R_{so}}{R_{sl}} \right)^{\frac{\pi v}{\delta}+1} \left(\frac{r}{R_{sl}} \right)^{\frac{\pi v}{\delta}-1} - \left(\frac{R_{so}}{r} \right)^{\frac{\pi v}{\delta}+1} \right] \cos\left[\dfrac{\pi v}{\delta} \left(\theta - \theta_j + \dfrac{\delta}{2} \right) \right] \end{array} \right. \tag{16}$$

where $R_{slm} = \sqrt{\left(R_{sl}^2 + R_{so}^2\right)/2}$ is the radius which radially divides each slot into two equal-area regions and

$$b_0^{so,j} = \frac{\mu_0}{2} \left[J_{b0}^j \left(R_{sl}^2 - R_{slm}^2 \right) + J_{t0}^j \left(R_{slm}^2 - R_{so}^2 \right) \right] \frac{\delta}{\beta} \tag{17}$$

The number of integration constants to be determined is $4N + Q(2U + V + 1) + 2pW$, consisting of a_n^a, b_n^a, c_n^a and d_n^a (for $n = 1, \ldots, N$), $a_u^{so,1}, \ldots, a_u^{so,Q}$ (for $n = 1, \ldots, U$), $b_u^{so,1}, \ldots, b_u^{so,Q}$ (for $n = 0, 1, \ldots, U$), $b_v^{sl,1}, \ldots, b_v^{sl,Q}$ (for $v = 1, \ldots, V$), and $a_w^{m,0}, \ldots, a_w^{m,2p-1}$ (for $w = 1, \ldots, W$) where N, V, U and W are the number of harmonics in the air-gap, slot, slot-opening and PM regions, respectively. The integral coefficients are obtained by imposing the boundary conditions at the interface between the various regions and are given in [31]. The analytical results of magnetic flux density components in the different subregions for 6-slots/4-poles Brushless PM machine with surface-inset PMs (for three magnetization patterns and non-overlapping winding) have been presented in [31] and evaluated by comparing them with those obtained from the FEM.

3. BACK EMF CALCULATION

The calculation of the magnetic flux linked with each coil due to only PMs is a prerequisite to compute the induced back EMF in each phase. The magnetic flux passing through a surface can be, in general, calculated by [5]

$$\phi = \int \mathbf{B} \cdot d\mathbf{S} \tag{18}$$

where $\mathbf{B}$ is the magnetic flux density vector distribution passing through the surface and $d\mathbf{S}$ an element of the surface area vector.

3.1. Non-Overlapping Winding

Using Gauss's law of magnetism of Maxwell's equations, $\oint \mathbf{B} \cdot d\mathbf{S} = 0$, the magnetic flux passing through one of the stator teeth, as shown in Figure 3(a), can be obtained by the following relation

$$\phi_{\mathrm{af}} = \int_{\mathbf{S}_{\mathrm{ab}}} \mathbf{B} \cdot d\mathbf{S} + \int_{\mathbf{S}_{\mathrm{bc}}} \mathbf{B} \cdot d\mathbf{S} + \int_{\mathbf{S}_{\mathrm{cd}}} \mathbf{B} \cdot d\mathbf{S} + \int_{\mathbf{S}_{\mathrm{de}}} \mathbf{B} \cdot d\mathbf{S} + \int_{\mathbf{S}_{\mathrm{ef}}} \mathbf{B} \cdot d\mathbf{S} \tag{19}$$

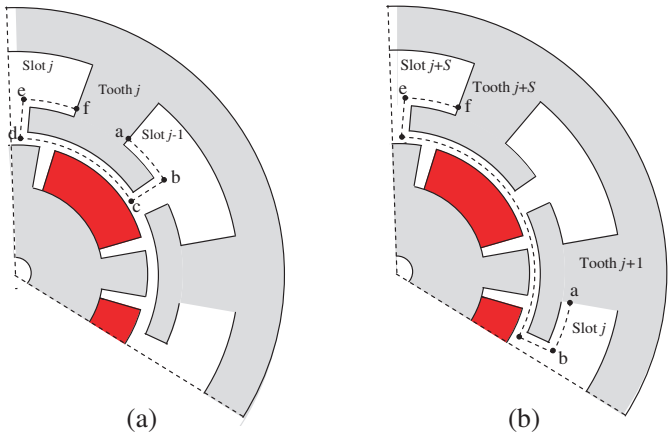

Figure 3. Winding layout of (a) 9-slots/8-poles BLDC machine with non-overlapping winding and (b) 15-slots/4-poles BLAC machine with overlapping winding.

For the sake of calculation ease, the integral surface is considered to be the surface around each tooth-tip. Therefore in the case of non-overlapping windings, the magnetic flux linked by a single turn of the j-th coil, i.e., the coil wound on the $(j+1)$-th tooth, is expressed by

$$\phi_j(\alpha) = L\cdot\left|\begin{array}{l} R_{so}\displaystyle\int_{\delta_{j+1}-(\theta_t-\delta+\beta)/2}^{\delta_{j+1}-\theta_t/2} B_r^{sl,j}\left(r,\theta',\alpha\right)\Big|_{r=R_{so}} d\theta' + \int_{R_{so}}^{R_s} B_\theta^{so,j}\left(r',\theta,\alpha\right)\Big|_{\theta=\delta_{j+1}-\theta_t/2} dr' \\ \ldots + R_s\displaystyle\int_{\delta_{j+1}-\theta_t/2}^{\delta_{j+1}+\theta_t/2} B_r^{a}\left(r,\theta',\alpha\right)\big|_{r=R_s} d\theta' + \int_{R_s}^{R_{so}} B_\theta^{so,j+1}\left(r',\theta,\alpha\right)\Big|_{\theta=\delta_{j+1}+\theta_t/2} dr' \\ \ldots + R_{so}\displaystyle\int_{\delta_{j+1}+\theta_t/2}^{\delta_{j+1}+(\theta_t-\delta+\beta)/2} B_r^{sl,j+1}\left(r,\theta',\alpha\right)\Big|_{r=R_{so}} d\theta' \end{array}\right. \tag{20}$$

for $j=1,2,\ldots,Q$ in the case of all teeth wound and $j=1,3,\ldots,Q$ in the case of alternate teeth wound where $\theta_t = 2\pi/Q-\beta$ is the span angle of each tooth including the tooth-tips, $\delta_j = 2\pi(j-1)/Q$ is the angle of j-th tooth center with respect to the first tooth, L is the effective axial length of the machine, and θ' & r' are dummy variables of integration. Using the analytical solution of magnetic flux density, the magnetic flux due to PM passing through tooth j is expressed as

$$\phi_j(\alpha) = L\cdot\left|\begin{array}{l} \displaystyle\sum_{v=1}^{V}\left[\left(\frac{R_{so}}{R_{sl}}\right)^{\frac{2\pi v}{\delta}}+1\right]\left\{\begin{array}{l} b_v^{sl,j}\left[\cos\left(\frac{\pi v}{\delta}\left(\frac{\beta}{2}+\frac{\delta}{2}\right)\right)-(-1)^v\right] \\ \ldots - b_v^{sl,j+1}\left[\cos\left(\frac{\pi v}{\delta}\left(-\frac{\beta}{2}+\frac{\delta}{2}\right)\right)-1\right]\end{array}\right\} \\ \ldots + \displaystyle\sum_{u=1}^{U}\left[\left(a_u^{so,j+1}-(-1)^u a_u^{so,j}\right)-\left(b_u^{so,j+1}-(-1)^u b_u^{so,j}\right)\right]\left[\left(\frac{R_s}{R_{so}}\right)^{\frac{\pi u}{\beta}}-1\right] \\ \ldots - 2L\displaystyle\sum_{n=1}^{N}\left\{\begin{array}{l}\left[a_n^a+b_n^a\left(\frac{R_m}{R_s}\right)^n\right]\sin\left(n\delta_{j+1}\right) \\ \ldots - \left[c_n^a+d_n^a\left(\frac{R_m}{R_s}\right)^n\right]\cos\left(n\delta_{j+1}\right)\end{array}\right\}\sin\left(n\theta_t/2\right)\end{array}\right. \tag{21}$$

Subsequently, the back EMF induced in coil j can be analytically found using Faraday's law [5]

$$E_j = -N_t \omega \frac{d\phi_j}{d\alpha} \tag{22}$$

where N_t is the number of turns of each coil. The back EMF of each phase can be obtained according to the connection of the coils of that phase.

3.2. Overlapping Winding

Similarly, using Gauss's law of magnetism of Maxwell's equations, the magnetic flux passing through the coil located in slots j and $j+S$, where S is the coil span in number of slots, as shown in Figure 3(b), can be obtained by the following relation

$$\phi_{\mathrm{j}} = \int_{\mathbf{S}_{\mathrm{ab}}} \mathbf{B}\cdot d\mathbf{S} + \int_{\mathbf{S}_{\mathrm{bc}}} \mathbf{B}\cdot d\mathbf{S} + \int_{\mathbf{S}_{\mathrm{cd}}} \mathbf{B}\cdot d\mathbf{S} + \int_{\mathbf{S}_{\mathrm{de}}} \mathbf{B}\cdot d\mathbf{S} + \int_{\mathbf{S}_{\mathrm{ef}}} \mathbf{B}\cdot d\mathbf{S} \tag{23}$$

Therefore in the case of overlapping windings, the magnetic flux linked by a single turn of the j-th coil, i.e., the coil located in slots j and $j+S$, is expressed by

$$\phi_j(\alpha) = L\cdot \left| \begin{array}{l} R_{so} \displaystyle\int_{\delta_{j+1}-(\theta_t-\delta+\beta)/2}^{\delta_{j+1}-\theta_t/2} B_r^{slt,j}\left(r,\theta',\alpha\right)\Big|_{r=R_{so}} d\theta' + \int_{R_{so}}^{R_s} B_\theta^{so,j}\left(r',\theta,\alpha\right)\Big|_{\theta=\delta_{j+1}-\theta_t/2} dr' \\ \ldots + R_s \displaystyle\int_{\delta_{j+1}-\theta_t/2}^{\delta_{j+S}+\theta_t/2} B_r^{a}\left(r,\theta',\alpha\right)\big|_{r=R_s} d\theta' + \int_{R_s}^{R_{so}} B_\theta^{so,j+S}\left(r',\theta,\alpha\right)\Big|_{\theta=\delta_{j+S}+\theta_t/2} dr' \\ \ldots + R_{so} \displaystyle\int_{\delta_{j+S}+\theta_t/2}^{\delta_{j+S}+(\theta_t-\delta+\beta)/2} B_r^{slt,j+S}\left(r,\theta',\alpha\right)\Big|_{r=R_{so}} d\theta' \end{array} \right. \tag{24}$$

for $j = 1, 2, \ldots, Q$. Using the analytical solution of magnetic flux density, the magnetic flux due to PM passing through coil j is expressed as

$$\phi_j(\alpha) = L\cdot \left| \begin{array}{l} \displaystyle\sum_{v=1}^{V}\left[\left(\frac{R_{so}}{R_{sl}}\right)^{\frac{2\pi v}{\delta}}+1\right]\left\{\begin{array}{l} b_v^{sl,j}\left[\cos\left(\frac{\pi v}{\delta}\left(\frac{\beta}{2}+\frac{\delta}{2}\right)\right)-(-1)^v\right] \\ \ldots - b_v^{sl,j+S}\left[\cos\left(\frac{\pi v}{\delta}\left(-\frac{\beta}{2}+\frac{\delta}{2}\right)\right)-1\right]\end{array}\right\} \\ \ldots + \displaystyle\sum_{u=1}^{U}\left[\left(a_u^{so,j+S}-(-1)^u a_u^{so,j}\right)-\left(b_u^{so,j+S}-(-1)^u b_u^{so,j}\right)\right]\left[\left(\frac{R_s}{R_{so}}\right)^{\frac{\pi u}{\beta}}-1\right] \\ \ldots - 2\displaystyle\sum_{n=1}^{N}\left\{\begin{array}{l}\left[a_n^a+b_n^a\left(\frac{R_m}{R_s}\right)^n\right]\sin\left(n\delta_{j+(S+1)/2}\right) \\ \ldots - \left[c_n^a+d_n^a\left(\frac{R_m}{R_s}\right)^n\right]\cos\left(n\delta_{j+(S+1)/2}\right)\end{array}\right\}\sin\left(n\pi\frac{S}{Q}-n\beta/2\right) \end{array} \right. \tag{25}$$

4. INDUCTANCES

Self-/mutual-inductances are calculated for both overlapping and non-overlapping winding configurations. The calculation is based on the armature flux linked with each coil which yields the self-inductance if the magnetic flux is generated by the coil current; and results in the mutual-inductances if the magnetic flux produces by another coil.

4.1. Non-Overlapping Winding

The flux linked with coil j (i.e., the coil wound on the $(j+1)$-th tooth) due to solely the current of coil j' can be obtained using the following expression

$$\lambda_{j,j'}(\alpha) = LN_t \left[\begin{array}{l} \sum_{v=1}^{V} \left[\left(\frac{R_{so}}{R_{sl}} \right)^{\frac{2\pi v}{\delta}} + 1 \right] \left\{ \begin{array}{l} b_v^{sl,j,j'} \left[\cos\left(\frac{\pi v}{\delta} \left(\frac{\beta}{2} + \frac{\delta}{2} \right) \right) - (-1)^v \right] \\ \ldots - b_v^{sl,j+1,j'} \left[\cos\left(\frac{\pi v}{\delta} \left(-\frac{\beta}{2} + \frac{\delta}{2} \right) \right) - 1 \right] \end{array} \right\} \\ \ldots + \sum_{v=1}^{V} \frac{\mu_0}{\left(\frac{\pi v}{\delta} \right)^2 - 4} \left[R_{so}^2 - \frac{2R_{sl}^2}{\frac{\pi v}{\delta}} \left(\frac{R_{so}}{R_{sl}} \right)^{\frac{\pi v}{\delta}} \right] \left\{ \begin{array}{l} J_v^{j,j'} \left[\cos\left(\frac{\pi v}{\delta} \left(\frac{\beta}{2} + \frac{\delta}{2} \right) \right) - (-1)^v \right] \\ \ldots - J_v^{j+1,j'} \left[\cos\left(\frac{\pi v}{\delta} \left(-\frac{\beta}{2} + \frac{\delta}{2} \right) \right) - 1 \right] \end{array} \right\} \\ \ldots + \left(b_0^{so,j+1,j'} - b_0^{so,j,j'} \right) \ln\left(\frac{R_s}{R_{so}} \right) \\ \ldots + \sum_{u=1}^{U} \left[\begin{array}{l} \left(a_u^{so,j+1,j'} - (-1)^u a_u^{so,j,j'} \right) \\ \ldots - \left(b_u^{so,j+1,j'} - (-1)^u b_u^{so,j,j'} \right) \end{array} \right] \left[\left(\frac{R_s}{R_{so}} \right)^{\frac{\pi u}{\beta}} - 1 \right] \\ \ldots - 2 \sum_{n=1}^{N} \left\{ \begin{array}{l} \left[a_n^{a,j'} + b_n^{a,j'} \left(\frac{R_m}{R_s} \right)^n \right] \sin(n\delta_{j+1}) \\ \ldots - \left[c_n^{a,j'} + d_n^{a,j'} \left(\frac{R_m}{R_s} \right)^n \right] \cos(n\delta_{j+1}) \end{array} \right\} \sin(n\theta_t/2) \end{array} \right] \tag{26}$$

for $j = 1, 2, \ldots, Q$ and $j' = 1, 2, \ldots, Q$ where $J_v^{j,j'}$ is the v-th component of the current density Fourier series in slot j when only coil j' is active. The integral constants are also calculated when only coil j' is carrying current without the effect of PMs. Having assumed the series connections of all coils in each phase, the self-inductance of phase k is calculated using the summation of the flux linked with the coils of phase k due to solely the corresponding coil current of phase k divided by the corresponding coil current of phase k

$$L_{k,k} = \sum_{j,j' \in k} \frac{\lambda_{j,j'}}{i_{j'}} \tag{27}$$

The mutual-inductance between phases k and k is calculated using the summation of the flux linked to the coils of phase k due to solely the coil current of phase k' divided by the coil current of phase k'

$$L_{k,k'} = \sum_{j \in k \& j' \in k'} \frac{\lambda_{j,j'}}{i_{j'}} \tag{28}$$

Since the permeability of the PMs is significantly lower than that of the iron interpoles in surface-inset PMs structures, regardless of having slotless or slotted stator, the armature field is a function of the rotor position and therefore self-/mutual-inductances vary with the rotor position.

4.2. Overlapping Winding

In the case of overlapping winding, the flux linked with coil j located between slot j and $j+S$ due to the current of coil j' is expressed as

$$\lambda_{j,j'}(\alpha) = LN_t \left[\begin{array}{l} \displaystyle\sum_{v=1}^{V} \left[\left(\frac{R_{so}}{R_{sl}} \right)^{\frac{2\pi v}{\delta}} + 1 \right] \left\{ \begin{array}{l} b_v^{sl,j,j'} \left[\cos\left(\frac{\pi v}{\delta} \left(\frac{\beta}{2} + \frac{\delta}{2} \right) \right) - (-1)^v \right] \\ \ldots - b_v^{sl,j+S,j'} \left[\cos\left(\frac{\pi v}{\delta} \left(-\frac{\beta}{2} + \frac{\delta}{2} \right) \right) - 1 \right] \end{array} \right\} \\ \ldots + \ln\left(\frac{R_s}{R_{so}} \right) \left[b_0^{so,j+S,j'} - b_0^{so,j,j'} \right] \\ \ldots + \displaystyle\sum_{u=1}^{U} \left[\begin{array}{l} \left(a_u^{so,j+S,j'} - (-1)^u a_u^{so,j,j'} \right) \\ \ldots - \left(b_u^{so,j+S,j'} - (-1)^u b_u^{so,j,j'} \right) \end{array} \right] \left[\left(\frac{R_s}{R_{so}} \right)^{\frac{\pi u}{\beta}} - 1 \right] \\ \ldots - 2 \displaystyle\sum_{n=1}^{N} \left\{ \begin{array}{l} \left[a_n^{a,j'} + b_n^{a,j'} \left(\frac{R_m}{R_s} \right)^n \right] \sin\left(n\delta_{j+S/2+1/2} \right) \\ \ldots - \left[c_n^{a,j'} + d_n^{a,j'} \left(\frac{R_m}{R_s} \right)^n \right] \cos\left(n\delta_{j+S/2+1/2} \right) \end{array} \right\} \sin\left(n\pi \frac{S}{Q} - n\beta/2 \right) \end{array} \right] \tag{29}$$

Note that in the case of alternate teeth wound or, in general, single layer windings, the number of coils is half of the number of slots. Therefore the flux linked with the coils is calculated for $j = 1, 3, \ldots, Q$. It is the case for both inductance and back EMF calculations.

5. TORQUE CALCULATION

Maxwell's theory is used to calculate the instantaneous torque; it states that the total force exerted on a rigid body located in an electromagnetic field is obtained by integrating the magnetic stress on a closed surface around the body [27].

$$T(t) = L \int_{-\pi}^{\pi} \frac{1}{\mu_0} \left(B_{r,PM}^a + B_{r,AR}^a \right) \left(B_{\theta,PM}^a + B_{\theta,AR}^a \right) \big|_{r=R_c} R_c^2 d\theta \tag{30}$$

where $B_{r,PM}^a$ and $B_{\theta,PM}^a$ are, respectively, the radial and tangential components of the flux density due to PMs in the air-gap, $B_{r,AR}^a$ and $B_{\theta,AR}^a$ are, respectively, the radial and tangential components of the flux density due to armature reaction in the air-gap and R_c is the radius of the closed surface in the air-gap. In this study, the integration surface is assumed to be a cylinder with the motor center and the radius of $R_c = (R_a + R_{sl})/2$. Opening the brackets of the integrand leads to the following expression

$$T(t) = \frac{LR_c^2}{\mu_0} \int_{-\pi}^{\pi} \left(B_{r,PM}^a B_{\theta,PM}^a + B_{r,AR}^a B_{\theta,PM}^a + B_{r,PM}^a B_{\theta,AR}^a + B_{r,AR}^a B_{\theta,AR}^a \right) \big|_{r=R_c} d\theta \tag{31}$$

The first term is solely originated from the PMs flux density and called cogging torque, which is normally generated due to the presence of stator slots and PMs. The last term is generated due to just the armature reaction flux density and known as reluctance torque, which is developed due to rotor saliency. The two middle terms are due to the interaction between the PMs and armature reaction fields. It means that the instantaneous developed torque has, in general, three components: reluctance, cogging and electromagnetic torques as written in the following

$$T(t) = T_{rel}(t) + T_{cog}(t) + T_{em}(t). \tag{32}$$

6. LOCAL TRACTION & UNBALANCED MAGNETIC FORCES

The radial and tangential magnetic local traction acting on the stator surface can be obtained based on the Maxwell stress tensor since the permeability of the stator/rotor back-iron assumed to be infinity [5]

$$f_r = \frac{1}{2\mu_0}\left(B_r^2 - B_\theta^2\right) \tag{33}$$

$$f_\theta = \frac{1}{\mu_0} B_r B_\theta \tag{34}$$

which can be transformed to Cartesian coordinates

$$f_x = f_r \cos\theta - f_\theta \sin\theta \tag{35}$$

$$f_y = f_r \sin\theta + f_\theta \cos\theta \tag{36}$$

The components of the UMFs exerted on the stator center are calculated over a circular surface normally in the middle of the air-gap region as

$$F_x(t) = \int_{-L/2}^{L/2}\int_{-\pi}^{\pi} f_x r d\theta dz = L\int_{-\pi}^{\pi} f_x r d\theta \tag{37}$$

$$F_y(t) = \int_{-L/2}^{L/2}\int_{-\pi}^{\pi} f_y r d\theta dz = L\int_{-\pi}^{\pi} f_y r d\theta \tag{38}$$

$$|F(t)| = \sqrt{F_x^2(t) + F_y^2(t)} \tag{39}$$

Note that the above expressions can be used to calculate the UMF due to only PMs (i.e., $B_r^a = B_{r,PM}^a$ and $B_\theta^a = B_{\theta,PM}^a$), the UMF due to solely armature reaction (i.e., $B_r^a = B_{r,AR}^a$ and $B_\theta^a = B_{\theta,AR}^a$) and the total UMF (i.e., $B_r^a = B_{r,PM}^a + B_{r,AR}^a$ and $B_\theta^a = B_{\theta,PM}^a + B_{\theta,AR}^a$).

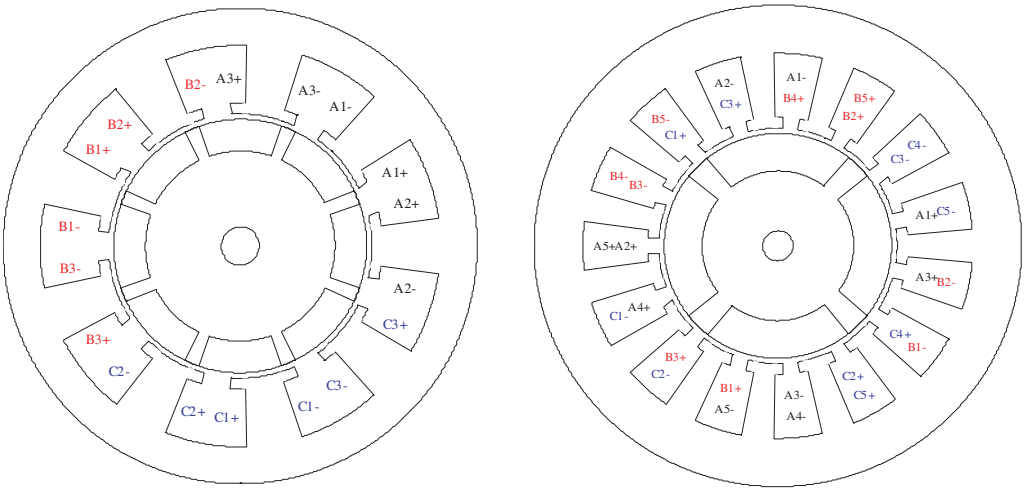

Figure 4. Winding layout of (a) 9-slots/8-poles BLDC machine with non-overlapping winding and (b) 15-slots/4-poles BLAC machine with overlapping winding.

7. CASE STUDIES

To illustrate the efficacy of the derived analytical expressions, two cases are investigated: a 9-slots/8-poles BLDC machine with non-overlapping winding and a 15-slots/4-poles BLAC machine with overlapping winding. The specifications of both cases are listed in Table 1 and their winding outlines are depicted in Figure 4. The 3-phases current waveforms for the two Brushless PM machines are shown in Figure 5.

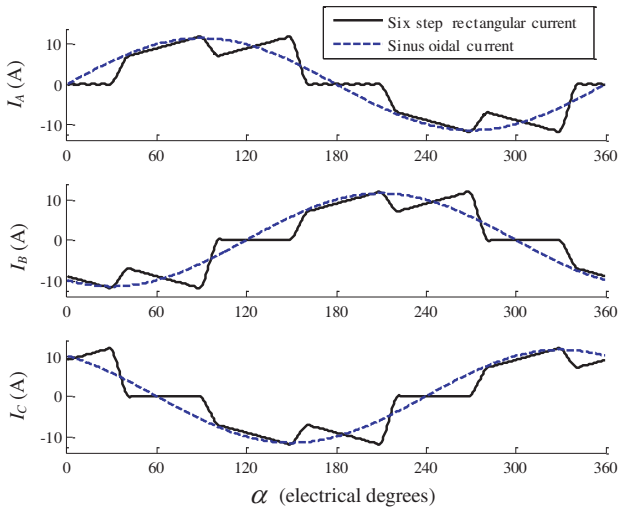

Figure 5. Current waveforms of the 3-phases Brushless PM machines.

Table 1. Specifications of the Brushless PM machines.

Parameters	Symbols (units)	9-slots/8-poles BLDC	15-slots/4-poles BLAC
Number of phases	q	3	3
Number of pole pairs	p	4	2
Number of slots	Q	9	15
Outer machine radius	R_o (mm)	45	45
Outer radius of the slots	R_{sl} (mm)	38	36
Outer radius of the slot-openings	R_{so} (mm)	27	24
Stator bore radius	R_s (mm)	25	22
PMs radius	R_m (mm)	24	21
Rotor back-iron radius	R_r (mm)	18	14
Effective axial length of the machine	L (mm)	100	100
Slot span angle	δ (rad)	0.419	0.251
Slot-opening span angle	β (rad)	0.209	0.126
PM pole-arc to pole-pitch ratio	α_p	0.85	0.85
Rotor back-iron groove arc to pole-pitch ratio	α_r	0.85	0.85
Remanent flux density of PMs	B_{rem} (T)	1	1
Relative magnetic permeability of PMs	μ_r	1.05	1.05
Number of turns in each phase	N_t	123	125
Magnetization pattern		Radial	Halbach
Currents waveform		Six-step rectangular	Sinusoidal
Number of harmonics in all subdomains	N, U, V, W	100	100

7.1. 9-Slots/8-Poles BLDC Machine

The Brushless PM machines with fractional ratio of slot number to pole number have some advantages over those with integer ratio such as low cogging torque. In addition, the non-overlapping winding reduces the end-winding which has no contribution to torque generation but increases the ohmic losses. In those machines where the number of slots and number of poles differ by one, i.e., $2p = Q \pm 1$, the back EMF and subsequently the torque is high since the coil pitch is close to pole-pitch.

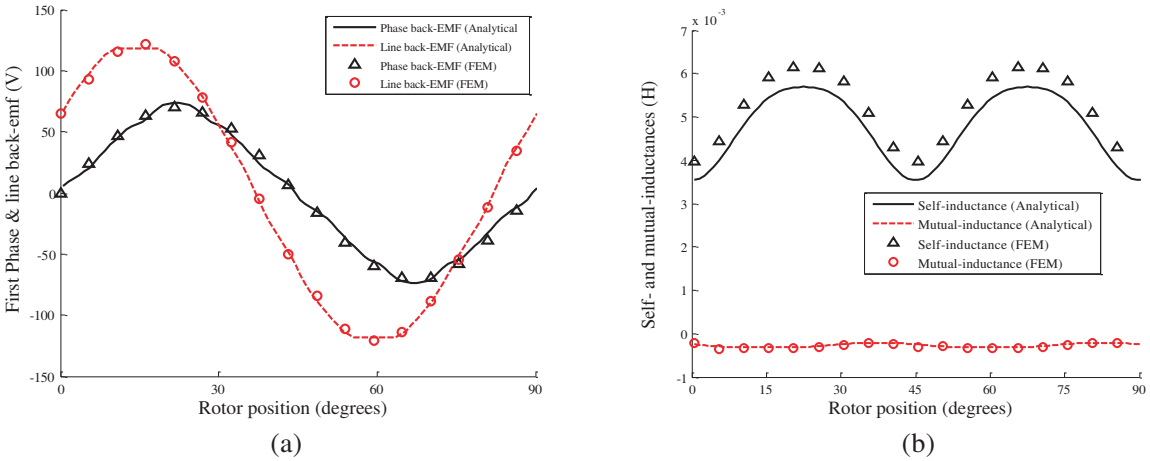

Figure 6. (a) Phase and line back EMF waveforms of the 9-slots/8-poles BLDC. (b) Self-/mutual-inductances of the 9-slots/8-poles BLDC machine.

The winding layout of the 9-slots/8-poles BLDC machine is shown in Figure 4(a). In this case, it is assumed that the PMs are radially magnetized and six-step rectangular armature currents flow in the armature winding.

Figure 6(a) shows the analytically calculated first phase and first line back EMF waveforms which compared to those obtained by the FEM. The self-/mutual-inductances of 9-slots/8-poles BLDC machine are depicted in Figure 6(b). Because of the rotor saliency, the inductances vary with rotor position.

Figure 7 shows the instantaneous developed torque which consists of three components: reluctance torque [see Figure 7(a)], cogging torque [see Figure 7(b)] and electromagnetic torque [see Figure 7(c)]. The minimum, maximum, average and ripple of the instantaneous torque are 5.07 Nm, 7.01 Nm, 6.31 Nm, and 30.78% respectively for six-step rectangular armature currents. For sinusoidal armature currents, the minimum, maximum, average and ripple of the instantaneous torque are 7.03 Nm, 7.34 Nm, 7.18 Nm, and 4.1% respectively.

The UMFs exerted on the rotor center along x- and y-axis as well as its modulus are shown in Figure 8(a). It is obvious that one of the disadvantages of the machines with a fractional slot number per pole number ratio is the developed UMFs which increase the vibration and acoustic noise and reduce the life time of the machine. Figure 8(b) shows the locus of the UMFs due to PM alone, due to just armature reaction (AR) and also the total UMFs, i.e., due to both PM and AR fields which incorporate their interactions.

7.2. 15-Slots/4-Poles BLAC Machine

The second case to be investigated is a 15-slots/4-poles BLAC machine with overlapping winding. The winding layout is selected to have a balanced winding with the coil pitch close to 180 electrical degrees, as shown in Figure 4(b).

The magnetization pattern, in this case, is Halbach and the armature current waveforms are assumed to be sinusoidal.

Similar to the previous case, the back EMF, self-/mutual-inductances, instantaneous torques, and UMFs have been analytically calculated. The induced back EMF waveforms in the first phase and first line are shown in Figure 9(a) in which the phase back EMF is more sinusoidal compared to that of the previous case. The rotor position dependent self-/mutual-inductances are depicted in Figure 9(b). Compared to that of the non-overlapping winding, the mutual-inductance is higher in the overlapping winding.

The instantaneous developed torque is shown in Figure 10. The torque ripple in this case is considerably lower compared to that of the BLDC motor. The minimum, maximum, average and ripple of the instantaneous torque are 6.7 Nm, 7.2 Nm, 6.89 Nm, and 7.77% respectively for six-step rectangular

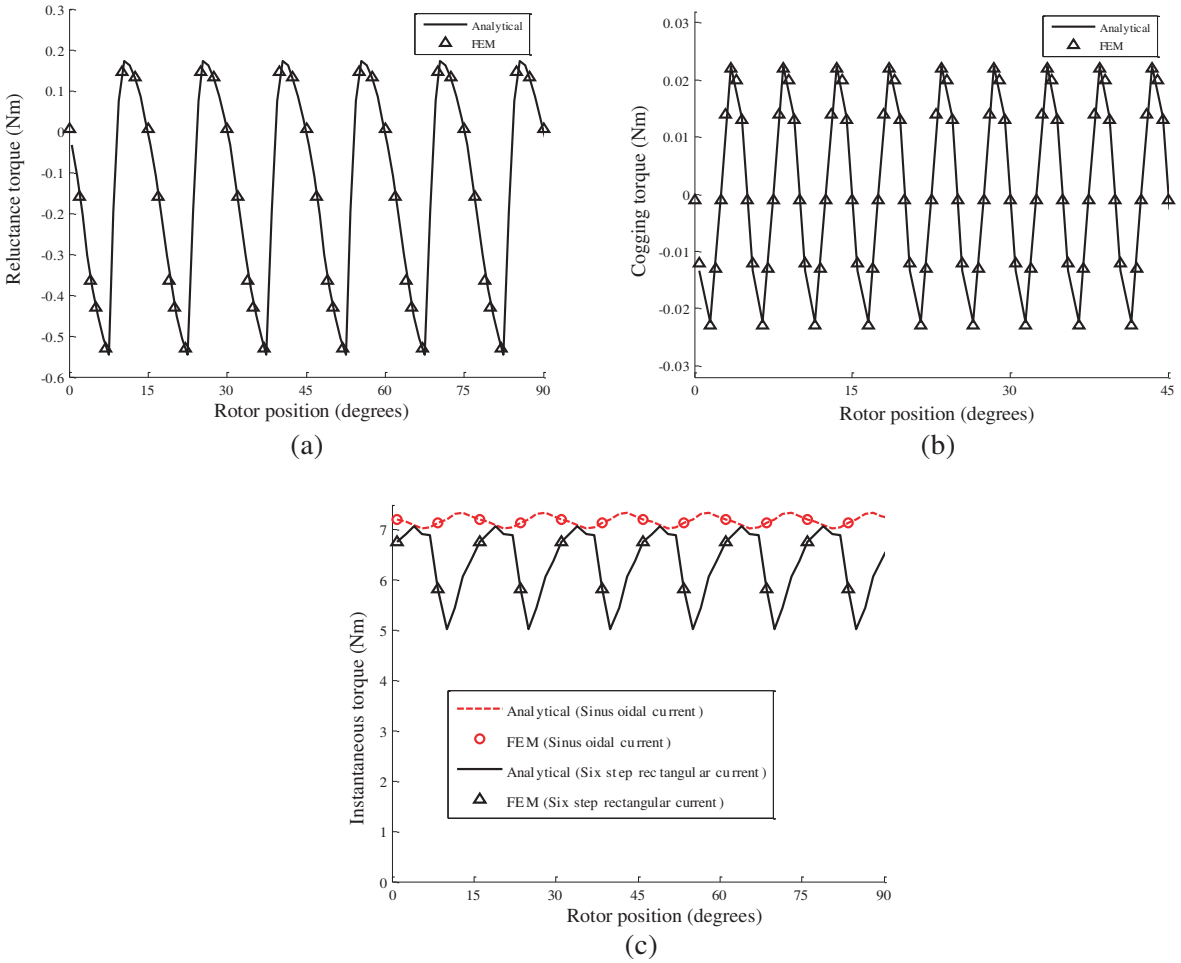

Figure 7. (a) Reluctance, (b) cogging and (c) instantaneous torques of the 9-slots/8-poles BLDC machine.

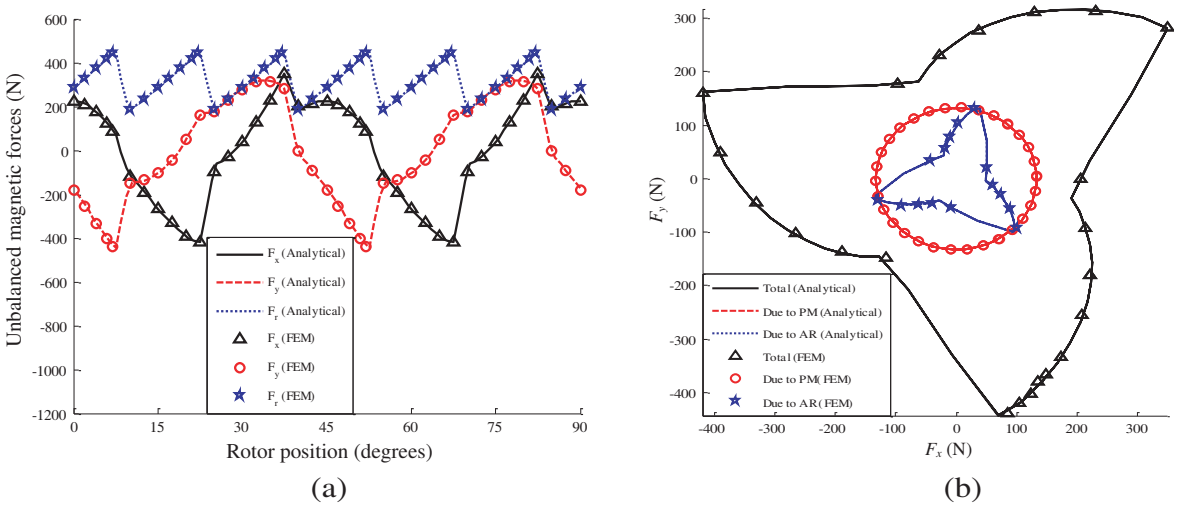

Figure 8. UMFs of the 9-slots/8-poles BLDC machine: (a) Waveforms, and (b) Locus.

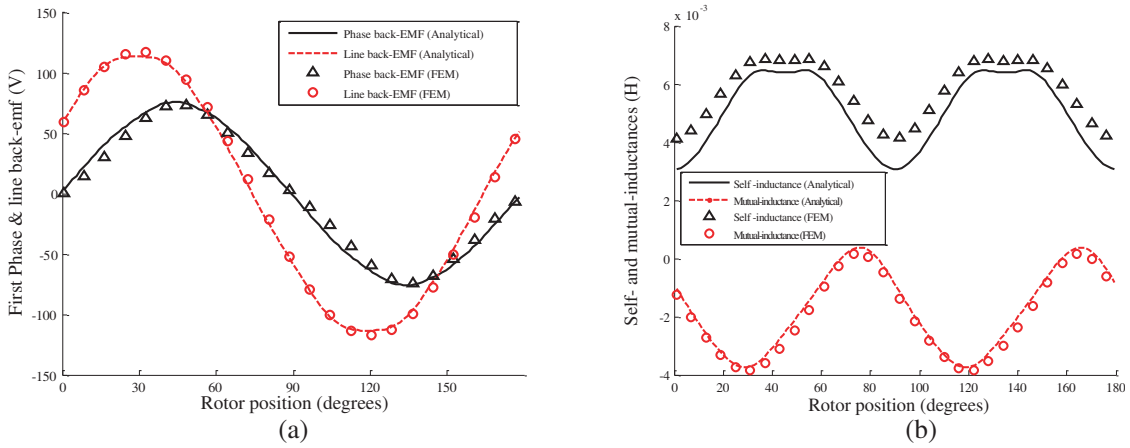

Figure 9. (a) Phase and line back EMF waveforms of the 15-slots/4-poles BLAC machine. (b) Self-/mutual-inductances of the 15-slots/4-poles BLAC machine.

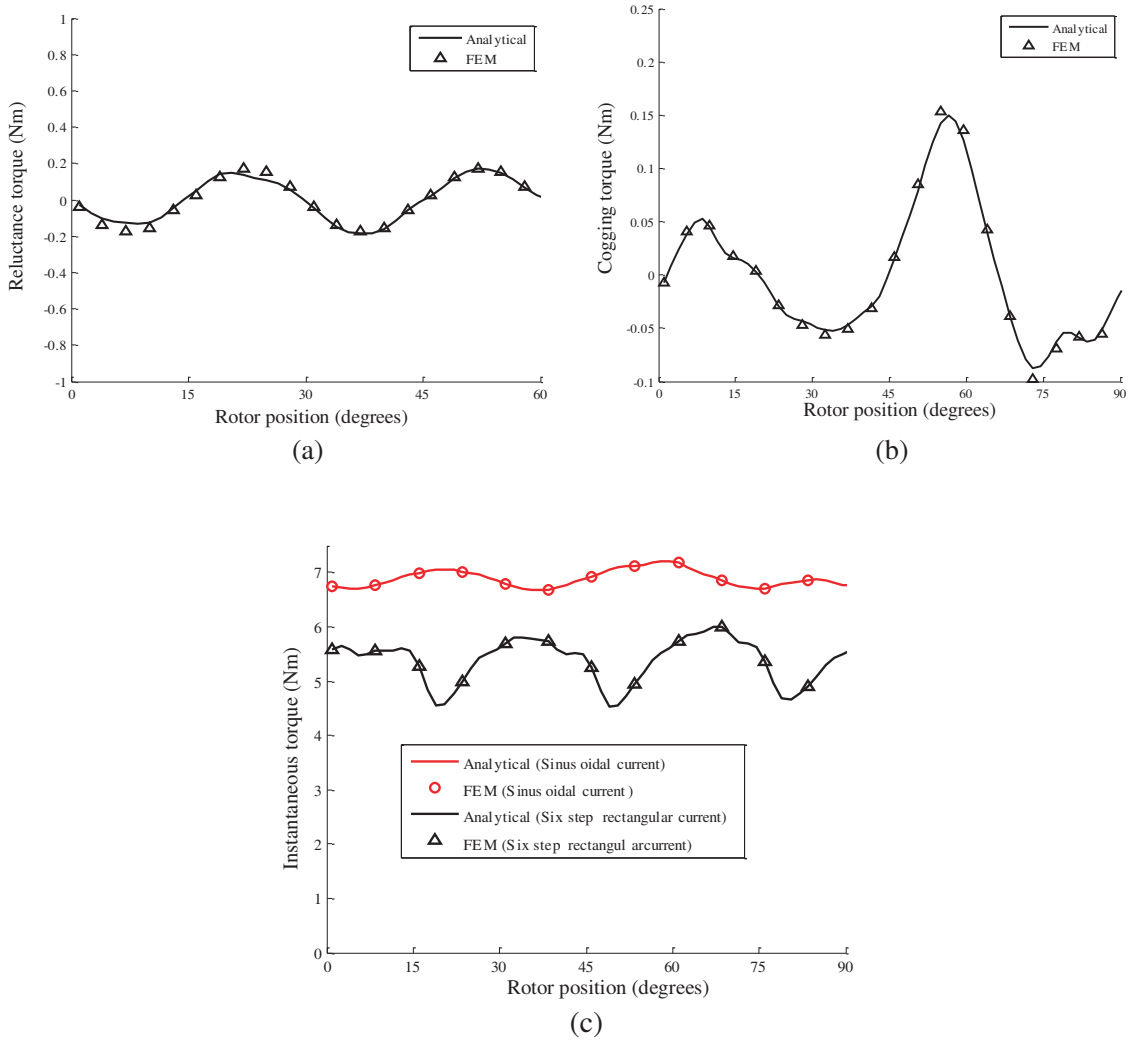

Figure 10. (a) Reluctance, (b) cogging and (c) instantaneous torques of the 15-slots/4-poles BLAC machine.

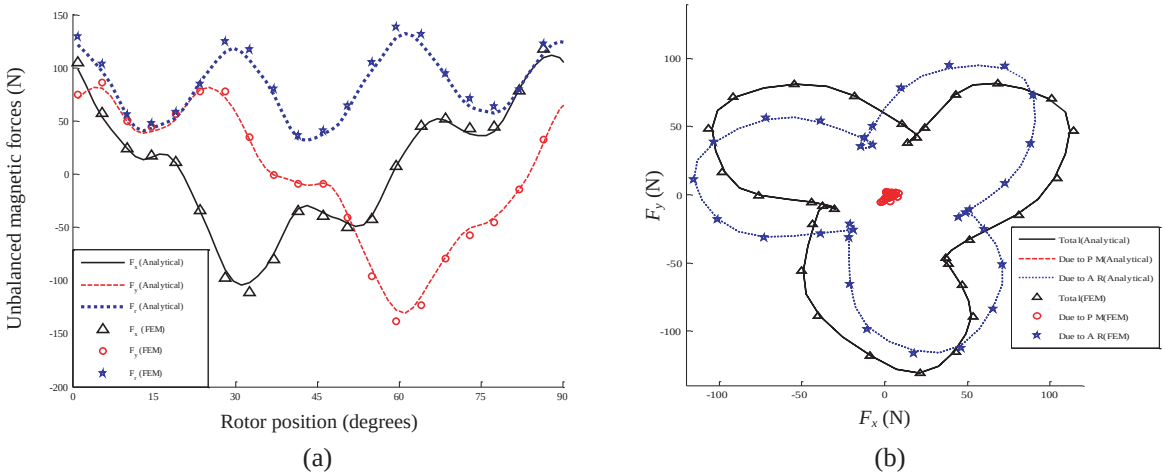

Figure 11. UMFs of the 15-slots/4-poles BLAC machine: (a) Waveforms, and (b) Locus.

armature currents. For sinusoidal armature currents, the minimum, maximum, average and ripple of the instantaneous torque are 4.53 Nm 6.01 Nm, 5.37 Nm, and 27.51% respectively.

Figure 11(a) shows the UMFs in x- and y-axis as well as the magnitude of UMF. The locus of the UMFs (i.e., F_x versus F_y) is shown in Figure 11(b) where the UMFs due to PM is negligible compared to the total UMFs because the Halbach array has been employed.

8. CONCLUSIONS

Analytical magnetic field distributions of Brushless machines with surface-inset PMs have been used to calculate important quantities such as back EMF, reluctance/cogging/instantaneous torques, self-/mutual-inductances, and the UMFs. These analytical expressions can facilitate the iterative design process of this type of PM machine. The analytical expressions have been tested on two cases: i) a 9-slots/8-poles BLDC machine with radially magnetized PMs, non-overlapping all teeth wound winding and six-step rectangular armature current waveforms; and ii) a 15-slots/4-poles BLAC machine with Halbach magnetization PMs, double-layer overlapping winding and sinusoidal armature current waveforms. The analytical results have been compared with those obtained by FEM and found to be in good agreement.

ACKNOWLEDGMENT

Portions of the work reported in this paper were funded by the Heptagon Fund, grant number QMUL-AD03; and portions were funded by the National Institute for Health Research (NIHR) Invention for Innovation (i4i) program (II-FS-0110-14076). The views expressed in this publication are those of the authors and not necessarily those of the NHS, the NIHR or the Department of Health. The motors discussed as examples in this paper are different from those designed for the products under development by the above grants.

REFERENCES

1. Zhu, Z. Q., D. Howe, and C. C. Chan, "Improved analytical model for predicting the magnetic field distribution in brushless permanent-magnet machines," *IEEE Trans. Magn*, Vol. 38, No. 1, 229–238, 2002.
2. Atallah, K., Z. Q. Zhu, D. Howe, and T. S. Birch, "Armature reaction field and winding inductances of slotless permanent-magnet brushless machines," *IEEE Trans. Magn.*, Vol. 34, No. 5, 3737–3744, 1998.

3. Holm, S. R., H. Polinder, and J. A. Ferreira, "Analytical modeling of a permanent-magnet synchronous machine in a flywheel," *IEEE Trans. Magn.*, Vol. 43, No. 5, 1955–1967, 2007.
4. Dubas, F., C. Espanet, and A. Miraoui, "Field diffusion equation in high-speed surface mounted permanent magnet motors, parasitic eddy-current losses," *Proc. Electromotion*, Lausanne, Switzerland, Sep. 2005.
5. Rahideh, A. and T. Korakianitis, "Analytical open-circuit magnetic field distribution of slotless brushless permanent magnet machines with rotor eccentricity," *IEEE Trans. Magn.*, Vol. 47, No. 12, 4791–4808, 2011.
6. Pfister, P.-D. and Y. Perriard, "Slotless permanent-magnet machines: General analytical magnetic field calculation," *IEEE Trans. Magn.*, Vol. 47, No. 6, 1739–1752, 2011.
7. Zarko, D., D. Ban, and T. A. Lipo, "Analytical calculation of magnetic field distribution in the slotted air gap of a surface permanent-magnet motor using complex relative air-gap permeance," *IEEE Trans. Magn.*, Vol. 42, No. 7, 1828–1837, 2006.
8. Liu, Z. J. and J. T. Li, "Analytical solution of air-gap field in permanent-magnet motors taking into account the effect of pole transition over slots," *IEEE Trans. Magn.*, Vol. 43, No. 10, 3872–3883, 2007.
9. Liu, Z. J. and J. T. Li, "Accurate prediction of magnetic field and magnetic forces in permanent magnet motors using an analytical solution," *IEEE Trans. Energy Convers.*, Vol. 23, No. 3, 717–726, 2008.
10. Liu, Z. J., J. T. Li, and Q. Jiang, "An improved analytical solution for predicting magnetic forces in permanent magnet motors," *Journal of Appl. Phys.*, Vol. 103, No. 7, 07F135, 2008.
11. Boughrara, K., B. L. Chikouche, R. Ibtiouen, D. Zarko, and O. Touhami, "Analytical model of slotted air-gap surface mounted permanent-magnet synchronous motor with magnet bars magnetized in the shifting direction," *IEEE Trans. Magn.*, Vol. 45, No. 2, 747–758, 2009.
12. Dubas, F. and C. Espanet, "Analytical solution of the magnetic field in permanent-magnet motors taking into account slotting effect: No-load vector potential and flux density calculation," *IEEE Trans. Magn.*, Vol. 45, 2097–2109, 2009.
13. Dubas, F., A. Sari, J. M. Kauffmann, and C. Espanet, "Cogging torque evaluation through a magnetic field analytical computation in permanent magnet motors," *Proc. ICEMS*, Tokyo, Japan, Nov. 2009.
14. Dubas, F. and C. Espanet, "Semi-analytical Solution of 2-D rotor eddy-current losses due to the slotting effect in SMPMM," *Proc. COMPUMAG*, Florianopolis, Brasil, Nov. 2009.
15. Zhu, Z. Q., L. J. Wu, and Z. P. Xia, "An accurate subdomain model for magnetic field computation in slotted surface mounted permanent magnet machines," *IEEE Trans. Magn.*, Vol. 46, No. 4, 1100–1115, 2010.
16. Wu, L. J., Z. Q. Zhu, D. Staton, M. Popescu, and D. Hawkins, "An improved subdomain model for predicting magnetic field of surface-mounted permanent-magnet machines accounting for tooth-tips," *IEEE Trans. Magn.*, Vol. 47, No. 6, 1693–1704, 2011.
17. Amara, Y., P. Reghem, and G. Barakat, "Analytical prediction of eddy-current loss in armature windings of permanent magnet brushless AC machines," *IEEE Trans. Magn.*, Vol. 46, No. 8, 3481–3484, 2010.
18. Lubin, T., S. Mezani, and A. Rezzoug, "2-D exact analytical model for surface-mounted permanent magnet motors with semi-closed slots," *IEEE Trans. Magn.*, Vol. 47, No. 2, 479–492, 2011.
19. Bellara, A., Y. Amara, G. Barakat, and B. Dakyo, "Two-dimensional exact analytical solution of armature reaction field in slotted surface mounted PM radial flux synchronous machines," *IEEE Trans. Magn.*, Vol. 45, No. 10, 4534–4538, 2009.
20. Wu, L. J., Z. Q. Zhu, D. Staton, M. Popescu, and D. Hawkins, "Subdomain model for predicting armature reaction field of surface-mounted permanent-magnet machines accounting for tooth-tips," *IEEE Trans. Magn.*, Vol. 47, No. 4, 812–822, 2011.
21. Rahideh, A. and T. Korakianitis, "Subdomain analytical magnetic field prediction of slotted brushless machines with surface mounted magnets," *Inter. Review of Elect. Eng.*, Vol. 7, No. 2,

3891–3909, 2012.

22. Gysen, B. L. J., K. J. Meessen, J. J. H. Paulides, and E. A. Lomonova, "General formulation of the electromagnetic field distribution in machines and devices using fourier analysis," *IEEE Trans. Magn.*, Vol. 46, No. 1, 39–52, 2010.
23. Boughrara, K., D. Zarko, R. Ibtiouen, O. Touhami, and A. Rezzoug, "Magnetic field analysis of inset and surface-mounted permanent-magnet synchronous motors using schwarz-christoffel transformation," *IEEE Trans. Magn.*, Vol. 45, No. 8, 3166–3178, 2009.
24. Rahideh, A. and T. Korakianitis, "Analytical magnetic field distribution of slotless brushless machines with inset permanent magnets," *IEEE Trans. Magn.*, Vol. 47, No. 6, 1763–1774, 2011.
25. Rahideh, A. and T. Korakianitis, "Analytical, armature reaction field distribution of slotless brushless machines with inset permanent magnets," *IEEE Trans. Magn.*, Vol. 48, No. 7, 2178–2191, 2012.
26. Zhu, Z. Q., D. Howe, and Z. P. Xia, "Prediction of open-circuit airgap field distribution in brushless machines having an inset permanent magnet rotor topology," *IEEE Trans. Magn.*, Vol. 30, No. 1, 98–107, 1994.
27. Rahideh, A., M. Mardaneh, and T. Korakianitis, "Analytical 2-D calculations of torque, inductance, and back-EMF for brushless slotless machines with surface inset magnets," *IEEE Trans. Magn.*, Vol. 49, No. 8, 4873–4884, 2013.
28. Dubas, F. and A. Rahideh, "2-D analytical PM eddy-current loss calculations in slotless PMSM equipped with surface-inset magnets," *IEEE Trans. Magn.*, Vol. 50, No. 3, Art. ID 6300320, 2014.
29. Jian, L., K. T. Chau, Y. Gong, C. Yu, and W. Li, "Analytical calculation of magnetic field in surface-inset permanent-magnet motors," *IEEE Trans. Magn.*, Vol. 45, No. 10, 4688–4691, 2009.
30. Lubin, T., S. Mezani, and A. Rezzoug, "Two-dimensional analytical calculation of magnetic field and electromagnetic torque for surface-inset permanent magnet motors," *IEEE Trans. Magn.*, Vol. 48, No. 6, 2080–2091, 2012.
31. Rahideh, A. and T. Korakianitis, "Analytical magnetic field calculation of slotted brushless PM machines with surface inset magnets," *IEEE Trans. Magn.*, Vol. 48, No. 10, 2633–2649, 2012.
32. Zarko, D., D. Ban, and T. A. Lipo, "Analytical solution for cogging torque in surface permanent-magnet motors using conformal mapping," *IEEE Trans. Magn.*, Vol. 44, No. 1, 52–65, 2008.
33. Zhu, Z. Q., D. Ishak, D. Howe, and J. Chen, "Unbalanced magnetic forces in permanent-magnet brushless machines with diametrically asymmetric phase windings," *IEEE Trans. Ind. Appl.*, Vol. 43, No. 6, 1544–1553, 2007.
34. Liang, Y., X. Bian, L. Yang, and L. Wu, "Numerical calculation of circulating current losses in stator transposition bar of large hydro-generator," *IET Sci., Meas. & Technol.*, Vol. 9, No. 4, 485–491, 2015.
35. Mohammed, O. A., S. Liu, and Z. Liu, "FE-based physical phase variable model of PM synchronous machines under stator winding short circuit faults," *IET Sci., Meas. & Technol.*, Vol. 1, No. 1, 12–16, 2007.
36. Clemens, M., J. Lang, D. Teleaga, and G. Wimmer, "Transient 3D magnetic field simulations with combined space and time mesh adaptivity for lowest order Whitney finite element formulations," *IET Sci., Meas. & Technol.*, Vol. 3, No. 6, 377–383, 2009.
37. Dubas, F. and K. Boughrara, "New scientific contribution on the 2-D subdomain technique in cartesian coordinates: Taking into account of iron parts," *Preprints (MDPI: Math. Comput. Appl.)*, 2016090106 (doi: 10.20944/preprints201609.0106.v1), 2016.